Modeling Radiation Damage Effects in 3D Pixel Digitization for the ATLAS Detector

Gilberto Giugliarelli, on behalf of the ATLAS Collaboration

University of Udine and INFN, Italy

Abstract

Silicon Pixel detectors are at the core of the current and planned upgrade of the ATLAS experiment at LHC. They constitute the part of ATLAS closest to the interaction point and for this reason they will be exposed – over their lifetime – to a significant amount of radiation: prior to the HL-LHC, the innermost layers will receive a fluence of 10^{15} n_{eq}/cm^2 and their HL–LHC upgrades will have to cope with an order of magnitude higher fluence integrated over their lifetimes. This poster presents the details of a new digitization model that includes radiation damage effects to the 3D Pixel sensors for the ATLAS Detector.

Keywords: 3D-Si sensors, ATLAS pixel upgrade, TCAD simulation

1. Introduction

The ATLAS inner detector [1, 2, 3] is devoted to the reconstruction of the tracks from charged particles. With the upgrade of the Large Hadron Collider (LHC), the extremely high radiation levels already present are expected to increase by a factor of ten (or more). The exposure of the sensors to radiation results in a signal loss due to the formation of defects in the silicon which act as traps for the charge generated by the passage of charged particles. As a result particle sensors and readout electronics [4] will require significantly increased radiation hardness.

3D silicon sensors were proposed (nearly two decades ago) as a more radiation tolerant alternative to traditional planar silicon sensors. In the 3D fabrication process, three-dimensional arrays of columns (etched into the silicon substrate) perpendicular to the detector surface constitute the electrodes of the 3D sensors (see Figure 1), rather than being implanted on top of it. With respect to the case of planar sensors, the 3D geometry allows to decouple inter–electrode distance from the sensitive device thickness and thus to strongly reduce the drift distance for the charges. The resulting reduction in collection times by an order of magnitude with respect to planar sensors significantly reduces the number of carriers that gets trapped in the sensor bulk. Moreover, the low inter–electrode distance allows for a reduction of the operational voltage and, therefore, for a lower power dissipation.

3D sensors are already in use in the ATLAS Insertable B-Layer (IBL) [2] and have performed well. These devices have a pixel size of 50×250 μm^2, where each pixel has two n+ columns shorted together with an inter–electrode distance of 67 μm etched into the 230 μm thick p–type silicon substrate. The radiation dose tolerance requirement on the 3D sensors currently in use is 5×10^{15} n_{eq}/cm^2 [2], while the typical expected fluence at the end of the operation of the HL–LHC is 1×10^{16} n_{eq}/cm^2.

This note focuses on modeling the non-ionizing energy losses in 3D sensors.

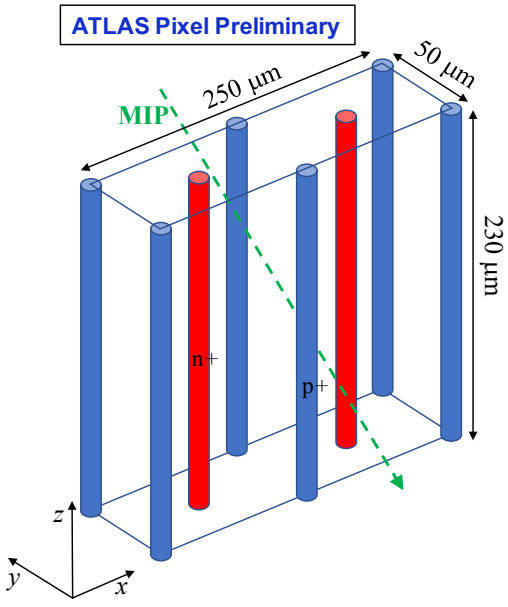

Figure 1: Electrodes geometry and dimensions for a 3D pixel. Red (blue) columns correspond to $n+$ ($p+$) electrodes; green dashed line is an example for the path of a minimum ionizing particle (MIP).

2. 3D pixel digitizer model

2.1. Particle hit and carrier motion

The passage of a minimum ionizing particle (MIP) through the silicon creates electrons and holes in the sensor. The sensor

Email address: gilberto.giugliarelli@cern.ch (Gilberto Giugliarelli, on behalf of the ATLAS Collaboration)

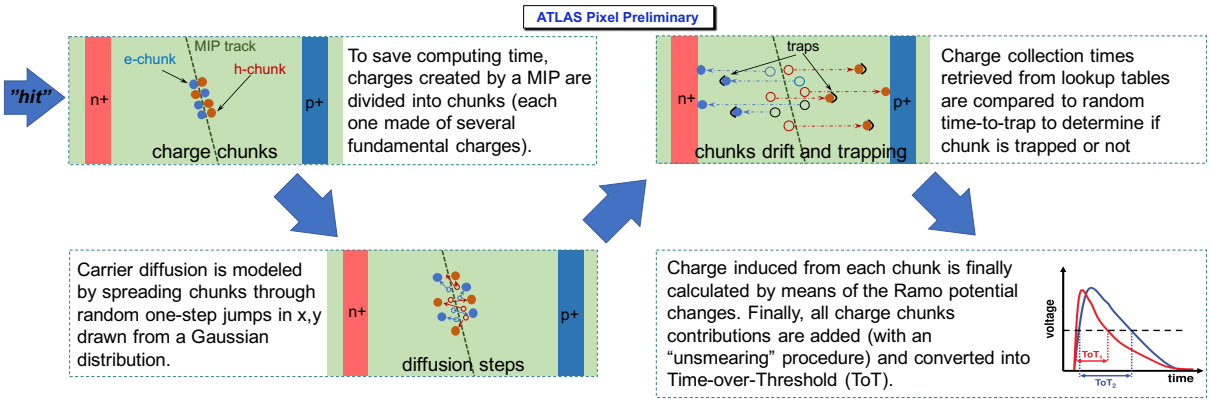

Figure 2: Schematic representation of the simulation process for the 3D pixel digitizer model.

is depleted and, because of the bias potential, the carriers drift towards the electrodes following the electric field lines. The geometry of 3D pixels is such that carriers drift toward the electrodes in the x-y plane parallel to the pixel (see Figure 1). Carriers motion is disturbed by thermal diffusion which gives rise to charge sharing between pixels when carriers diffuse into neighboring pixels and thus generate a signal in a pixel different from where they were created. This effect is modeled by displacing the charges through random one–step jumps in x and y drawn from a Gaussian distribution where the diffusion length standard deviation is given by

$$\sigma = \sqrt{\frac{2\mu(E)k_B T \cdot t}{q}}, \tag{1}$$

where q denotes the absolute value of the electron charge, $\mu(E)$ the electric field–dependent mobility, k_B the Boltzmann constant, T the temperature and t the time the carrier spends drifting.

In the absence of radiation damages all carriers generated from a MIP will reach (sooner or later) an electrode. The expected time one carrier would take to reach an electrode can be obtained by the following integral:

$$t_{el} = \int_{P_0}^{n+,p+} \frac{1}{\mu^{e,h}(E)E} ds, \tag{2}$$

calculated over the carrier path from the position where the carrier was created $P_0 = (x_0, y_0)$ to the final electrode ($n+$ or $p+$ depending on the electron/hole nature of the carrier). The previous expression comes from the integration of the equation of motion over the drift path using the drift velocity $v_{drift} = \pm\mu^{e,h}(E)E$. The corresponding carrier-dependent mobility $\mu^{e,h}$ is parametrized by the electric field E and temperature [5].

2.2. Radiation damage

On the contrary, in the presence of radiation damage, the carriers may be trapped somewhere. We have simulated this process by considering an exponential distribution for the trapping times with mean value $1/\kappa\Phi$ where the constant $\kappa = 3 \times 10^{-16}$ cm^2/ns is experimentally determined [6] and Φ is the integrated radiation fluence.

2.3. Calculation of the induced charge

While the carriers move inside the sensor, their movement induce a current on the neighboring collecting electrodes (n+ electrodes) and this process gives rise to a signal regardless of whether they reach an electrode or not. The amount of charge induced to each collecting electrode can be calculated by using a geometry–dependent potential referred to as the Ramo Potential ϕ [7, 8]. The charge induced by a carrier at position (x, y) after having drifted along a path starting at initial location (x_0, y_0) will be the difference in Ramo Potential $\Delta\phi$ between these two positions multiplied by the elementary carrier charge q, so that

$$q_{ind} = -q\Delta\phi = -q\left[\phi(x, y) - \phi(x_0, y_0)\right]. \tag{3}$$

2.4. Charge chunks and unsmearing

The number of electron–hole pairs created by a MIP is ~ 80 per micron. For efficient digitization, the motion of each fundamental charge cannot be treated separately, instead the charge deposited in each hit is divided into *chunks* composed of several fundamental charges and collectively propagated through the sensor. Such a simplification does not have an impact on the average amount of induced charge $\langle Q\rangle$, but can produce enlarged fluctuations. This can be compensated with an *unsmearing* procedure consisting of a correction to account for the fact that the charge chunks are not fundamental according to

$$Q \to Q + \frac{1}{\sqrt{n}}\left(Q - \langle Q\rangle\right). \tag{4}$$

The correction factor scales with the number of electron-hole pairs in the chunk n. Therefore, the average charge induced by the collection of particles starting out at position (x_0, y_0) can be obtained by integrating the equation of motion. As electrons and holes drift along the electric field lines towards $n+$ and $p+$ electrodes respectively, we have

$$\langle Q\rangle = qn\left(\int_{P_0}^{n+} p^{(e)}[(x_0, y_0) \to (x, y)][\phi(x, y) - \phi(x_0, y_0)]\mathrm{d}s - \right.$$
$$\left. - \int_{P_0}^{p+} p^{(h)}[(x_0, y_0) \to (x, y)][\phi(x, y) - \phi(x_0, y_0)]\mathrm{d}s\right) \tag{5}$$

where $p^{(e),(h)}[(x_0, y_0) \rightarrow (x, y)]$ is the probability of the carrier to reach point (x, y) before getting trapped.

2.5. ToT and digitizing

Finally, the charge collected for each pixel is converted to the time–over–threshold (ToT).

The above simulation model has been implemented in the ATLAS simulation framework. A schematic representation of the whole simulation process is summarized in Figure 2.

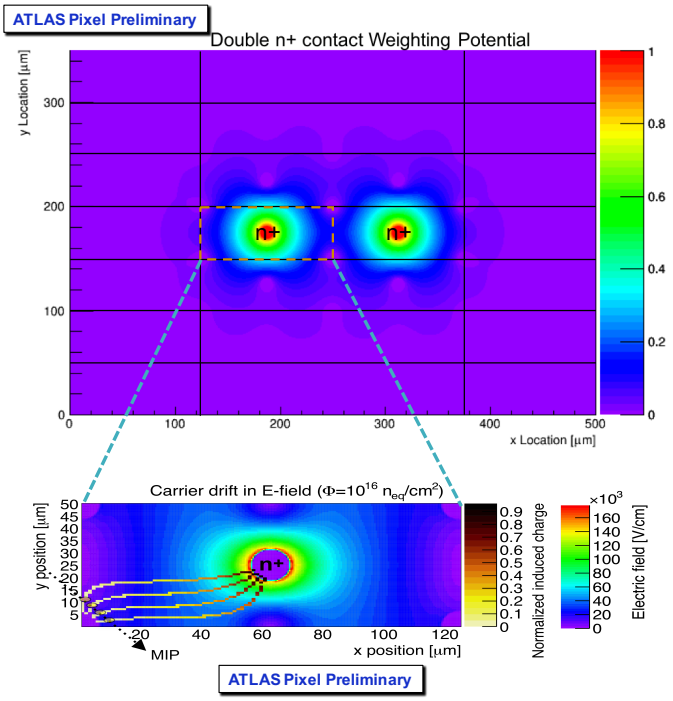

Figure 3: Top: Ramo potential; it can be noted how the potential spreads also to the neighboring pixels. Bottom: Average fraction of induced charge from electron at different trapping locations.

3. TCAD simulations

The implementation of the model described in the previous section requires the use of Ramo potential and electric field maps for the sensor. These maps are obtained by means of Technology Computer-Aided Design (TCAD) simulations. The two–dimensional map of the Ramo potential is shown in Figure 3; the picture clearly shows how the potential extends also to neighboring pixels. Electric field maps have to be recalculated for each different level of irradiation and have been obtained by using the radiation damage Perugia model [9]. Examples of these maps for unirradiated and high fluence cases are shown in Figure 4. The different values of fluences Φ considered in this study and the corresponding bias voltages V_{bias} to model full depletion are listed in Table 1.

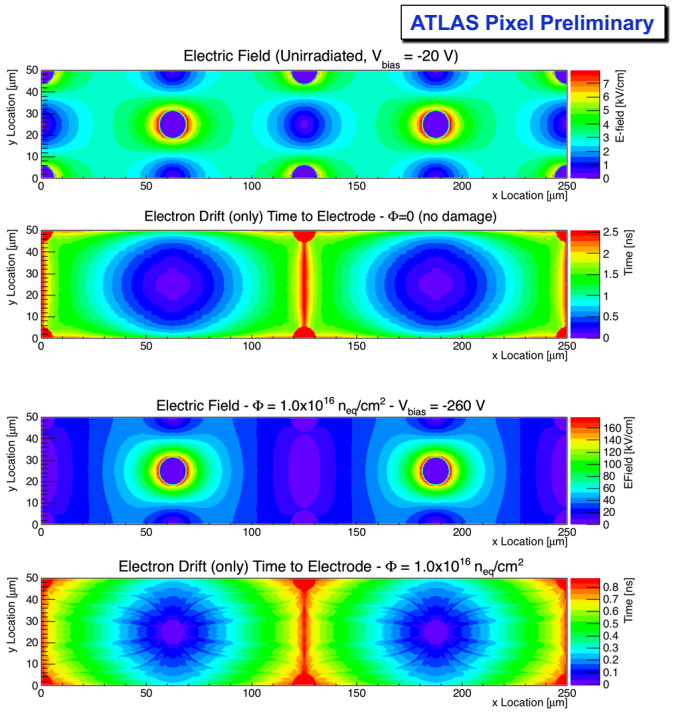

Figure 4: Top: electric field and corresponding time to electrode maps for an unirradiated pixel sensor; Bottom: electric field and corresponding time to electrode maps for a fluence $\Phi = 10^{16}$ n_{eq}/cm^2.

Table 1: Simulated fluences and corresponding bias voltages.

Φ [n_{eq}/cm^2]	V_{bias} [V]
1×10^{14}	-20
2×10^{14}	-30
5×10^{14}	-40
1×10^{15}	-50
2×10^{15}	-80
5×10^{15}	-160
6×10^{15}	-190
1×10^{16}	-260

The expected times to reach the electrode for electrons and holes, respectively, can easily be pre-calculated from electric field data according to equation (2). To speed up the digitizer performance, these data are stored in histograms and used as lookup tables to quickly be retrieved for any initial position within the pixel. Example of these maps are shown in Figure 4.

4. An alternative digitizer approach

In the standard approach to digitization (the one described in section 2.4) the use of charge chunks is essential to obtain reasonable simulation times. This approach has the drawback that charge chunk correction must be applied for every hit. We developed an alternative approach in which the use of specific pre–calculated maps for the induced charge chunks as lookup tables allows for a significant simplification in the digit-

izer structure and, consequently, to a consistent reduction in the simulation times.

We have considered a simulation in which the fundamental charges belonging to charge chunks with different sizes n and starting pixel positions were fully propagated through the sensor. The analysis of the results of these simulations allowed us to verify that the chunk induced charges Q_n are normally distributed variables with mean values $\langle Q_n \rangle$ and standard deviations σ_{Q_n} proportional to n and $n^{1/2}$, respectively. The proportionality constants between n and $\langle Q \rangle_n$ and $n^{1/2}$ and σ_{Q_n} depends only on the starting position of each chunk and can be extracted by an accurate calculation of the chunk induced charge maps for a specific chunk size (see an example in Figure 5). The use of these maps as lookup tables in the digitizer, allows one to *reconstruct* very quickly (and without making any charge propagation again) the induced charge associated to any chunk of any size and then to any MIP path through the sensor. Note also that in such a case, no other lookup tables are needed in the digitizer.

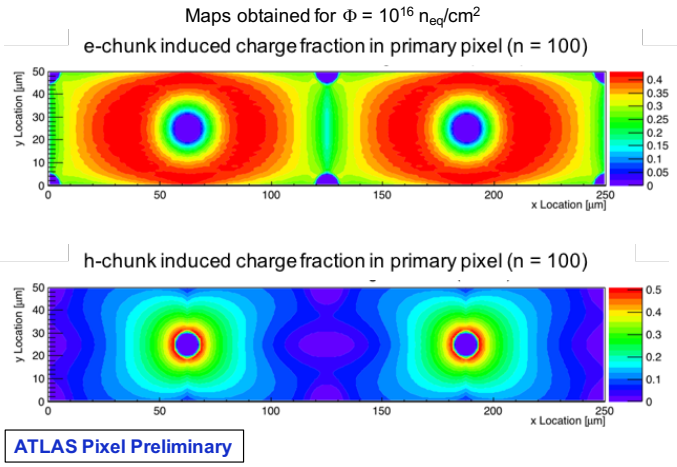

Figure 5: An example of the maps for the chunk induced charge fraction in the primary pixel for electron and hole chunks of size $n = 100$ and fluence $\Phi = 1 \times 10^{16}$ n_{eq}/cm^2.

We are completing the tests of the performances of this alternative approach; the results are very promising and soon we will integrate it in the ATLAS simulation framework.

5. Results and conclusions

The 3D digitizer for the ATLAS detector at HL-LHC is under testing and we started to compare its predictions with those of its planar counterpart and, when possible, with test beam data.

As an example, we consider the calculation of the ratio between the charge collected before and after irradiation which is usually referred to as the charge collection efficiency (CCE). This parameter provides a measure of the signal loss and performance degradation during the detector lifespan. In Figure 6 we show a comparison between the CCE as obtained by means of the 3D digitizer model (left panel) and those from existing test beam data (right panel). The figure shows a very good agreement between the two.

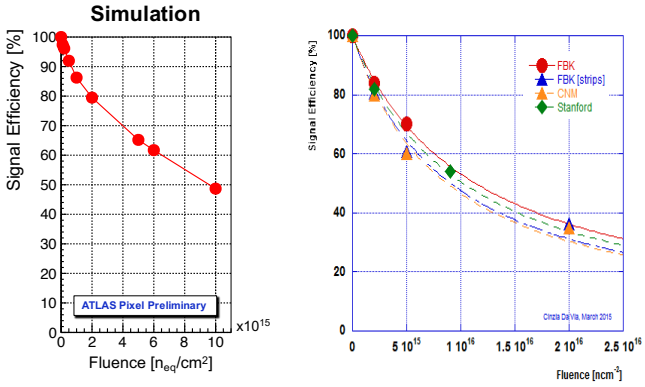

Figure 6: Left: charge collection efficiency (CCE) for different fluences obtained with 3D pixel digitizer model. Right: CCE from existing test beam data ([10]).

Summarizing, the 3D digitizer we have implemented allows for a very accurate evaluation of the induced charge in pixels taking into account radiation damage effects. Charge sharing effects are also included in the model and fluctuations caused by charge chunks are very accurately treated. Finally, original strategies have been developed to speed up the simulations.

References

[1] ATLAS Collaboration, *The ATLAS Experiment at the CERN Large Hadron Collider*, JINST **3** S08003 (2008).

[2] ATLAS Collaboration, *ATLAS Insertable B-Layer Technical Design Report*, tech. rep CERN-LHCC-2013. ATLAS-TDR-19.

[3] G. Aad et al., *ATLAS pixel detector electronics and sensors*, JINST **3** (2008) P07007.

[4] ATLAS Collaboration, *Technical Design Report for the ATLAS Inner Tracker Strip Detector* (2017) [CERN-LHCC-2017-005].

[5] C. Jacoboni et al., *A review of some charge transport properties of silicon*, Solid–State Electronics **20** 77 (1977).

[6] G. Alimonti et al., *A study of charge trapping in irradiated silicon with test beam data*, ATL-INDET-2003-014 (2003) [cds.cern.ch:685542].

[7] S. Ramo, *Current Induced by Electron Motion*, Proc. IRE **27** (1939) 584.

[8] W. Shockley, *Currents to Conductors Induced by a Moving Point Charge*, J. App. Phys. **9** (1938) 635.

[9] F. Moscatelli et al., *Combined Bulk and Surface Damage Effects at Very High Fluences in Silicon Detectors: Measurements and TCAD Simulations*, IEEE Transactions on Nuclear Science **63** (2016) 2716.

[10] G.-F. Dalla Betta, *3D Silicon Detectors*, Proceedings of The 1st INFN Workshop on Future Detectors for LHC, PoS (IFD2014) 013